Design of LLC Magnetically Integrated Transformer based on Nanocrystalline Soft Magnetic Composite Leakage Core

Kaimeng Shi, Dianhai Zhang, Xuanzhe Zhao, and Ziyan Ren

***Abstract*—Magnetic integration technology can reduce the printed circuit board (PCB) size of inductor-inductor-capacitor (LLC) converters. However, conventional methods for adjusting leakage inductance by modifying the transformer's air gap exhibit low sensitivity and limited output power capability. This paper proposes a novel magnetically integrated transformer structure that employs nanocrystalline soft magnetic composite (SMC) lamination to separate primary and secondary cores. Using SMC for the leakage core allows for more precise control of the magnetic flux division, enabling accurate leakage inductance tuning. Furthermore, this design achieves a higher magnetizing inductance per turn. Experimental results show that the proposed GU30 magnetically integrated transformer handles a primary input active power of 206.9 W, outperforming conventional designs while maintaining a full-load efficiency above 95%. This technology has the potential to further enhance the power density of power conversion products.**

***Index Terms*—Soft magnetic composite (SMC), Magnetic integration technology, High frequency transformer, LLC resonant converter.**

I. INTRODUCTION

As power electronic equipment evolves toward higher frequency and power density, traditional discrete magnetic components face challenges such as large volume, high loss, and significant electromagnetic interference (EMI). The integrated design of transformers and magnetic components, such as inductors through magnetic integration technology, can significantly reduce the system's size, optimize the flux distribution, suppress the noise, improve the electromagnetic compatibility (EMC) characteristics, etc. [1]-[3]. This innovative design has broad application prospects in space- and efficiency-sensitive fields such as energy storage systems, new energy on-board chargers (OBCs), megawatt-class charging piles, and data center power supplies [4]-[6]. Furthermore, in-depth research on magnetically integrated transformers and their losses will advance the application of novel magnetic materials and three-dimensional magnetic circuit design. This provides new technical pathways for improving the efficiency of power electronic devices [7]-[9].

In recent years, magnetically integrated transformers have been widely studied in resonant converters as a key technology to enhance the power density and efficiency of power electronic converters [10]-[12]. Current research mainly focuses on topology optimization, transformer winding design, and transformer core structure design to efficiently integrate multiple magnetic components [13]-[15]. However, the magnetic integration technology still faces challenges: First, the core loss and winding skin effect increase at high frequencies, requiring the use of new materials or three-dimensional magnetic circuit optimization design; second, it is difficult to ensure the consistency of the processing of complex core structures, affecting the symmetry of the parameters; and third, the leakage inductance regulation due to multiphase coupling still requires fine design. In resonant converter topologies such as inductor-inductor-capacitor (LLC) and capacitor-inductor-inductor-capacitor (CLLC), high-frequency transformers must work with resonant inductors and capacitors to realize soft switching of switching tubes and thus improve system efficiency [16]-[17]. A key challenge in magnetic integration design is achieving leakage inductance parameters with a wide and controllable range.

A limitation of the conventional air-gap width adjustment method is that the leakage inductance is relatively insensitive to structural parameter changes. This nonlinearity hinders the miniaturization of power electronic devices [18]. In addition, since the leakage flux path is mainly distributed in the windings adjacent to the air gap, it leads to additional eddy current losses on the transformer, which reduces the overall efficiency of the converter system. The leakage flux leaking into the air may cause the high-frequency transformer to couple with other magnetic components (e.g., power factor correction (PFC) inductors, etc.), resulting in a failed EMI test. References [19]-[20] utilized thin-film magnetic materials such as IFL04 or Fair-Rite M6 (Fair-Rite Corporation) as leakage

Manuscript received July 06, 2025; revised August 20, November 02 and December 02, 2025; accepted December 08, 2025. Date of publication December 25, 2025; Date of current version December 12, 2025.

This work was supported in part by the National Natural Science Foundation of China under Grant 51707125 and in part by the Scientific Research Project of Liaoning Provincial Department of Education under Grant LJKZ0125.

Kaimeng Shi, Dianhai Zhang, Xuanzhe Zhao, and Ziyan Ren are with Key Lab of Special Electric Machine and High Voltage Apparatus (Shenyang University of Technology), Ministry of Education, Shenyang 110870, China (e-mail: dr.shikaimeng@smail.sut.edu.cn; zhangdh@sut.edu.cn; zhaoxz@smail. sut. edu.cn; zyren@sut.edu.cn).

(*Corresponding Author*: *Dianhai Zhang*)

Digital Object Identifier 10.30941/CESTEMS.2025.00039

cores and demonstrated promising experimental performance. However, the limited formability of film material restricts its design freedom.

Soft magnetic composite (SMC) is a composite of magnetic powder and insulating material, which combines excellent high-frequency characteristics and tunable magnetic properties while supporting complex three-dimensional structure design [21]-[22]. Reference [23] describes the correlation between the magnetic properties of nanocrystalline SMC and its production process parameters (magnetic powder size, magnetic core density, and binder ratio). It demonstrates the potential application of nanocrystalline powder in power electronic devices.

This paper proposes a novel magnetically integrated transformer structure based on nanocrystalline SMC leakage inductance cores. Since the permeability of SMC can be precisely controlled during its fabrication, this approach addresses the issue of insensitive leakage inductance adjustment in conventional structures while simultaneously enhancing the transformer's output power. The paper details the methodology for regulating SMC permeability and the structural design of the magnetically integrated transformer, with prototype experiments validating the effectiveness of the proposed method.

II. LLC Magnetically Integrated Transformer Design

A. Magnetic Integration Principles and Methods

Fig. 1 shows the topology of the LLC resonant converter. The so-called magnetic integration integrates the resonant inductor into the main transformer to reduce the converter's overall size. Since the magnetic flux in the resonant inductor is not coupled to the transformer's secondary winding, magnetic integration can be achieved by artificially adding the transformer leakage circuit.

This study uses a GU series pot-core ferrite, with primary and secondary windings wound separately. The main flux path uses ferrite, while the leakage flux path uses SMC, as shown in Fig. 2(a). Part of the magnetic flux generated by the primary winding links with itself through the leakage core, while the remaining flux crosses the leakage core and returns via the transformer sidewalls, thereby coupling the primary and secondary windings.

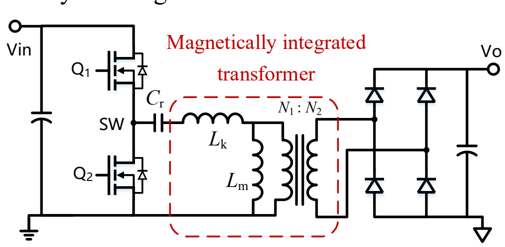

Fig. 1. Half-bridge LLC resonant converter topology.

Designing an LLC resonant converter typically requires adjusting the ratio of magnetizing inductance to resonant inductance to optimize performance. In this paper, the transformer leakage inductance is the resonant inductance. Using SMC as the leakage core material allows precise tailoring of its permeability through adjustments in the preparation process, enabling accurate control of both resonant and magnetizing inductance.

B. Qualitative Analysis of Leakage Inductance

The magnetic circuit model of the magnetically integrated transformer proposed in this study is shown in Fig. 2(b). Its leakage inductance L_k and leakage flux Φ_k are calculated as (1) and (2), respectively:

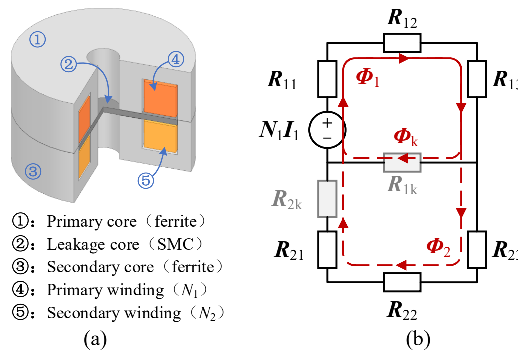

Fig. 2. Structure of the proposed integrated transformer. (a) Transformer profile structure. (b) Transformer equivalent magnetic circuit.

$$L_k = \frac{\Phi_k N_1}{I_1} \tag{1}$$

$$\Phi_k = \frac{N_1 I_1}{R_1 + \dfrac{R_{1k} R_2}{R_{1k} + R_2}} \cdot \frac{R_2}{R_{1k} + R_2} \tag{2}$$

where N_1 and I_1 denote the number of turns and the current of the primary winding, respectively. Among them, R_{11}, R_{12}, and R_{13} are referred to as the magnetic reluctances of the three parts of the primary magnetic core, and R_1 is referred to as the sum of the magnetic reluctances of these three parts. R_{21}, R_{22}, and R_{23} are referred to as the magnetic reluctance of the three parts of the secondary magnetic core, while R_{1k} and R_{2k} are respectively referred to as the leakage magnetic reluctance of the primary and secondary magnetic circuits and R_2 is the sum of the magnetic reluctance of the three parts of the secondary magnetic core and the leakage magnetic reluctance R_{2k}.

$$\begin{cases} R_1 = R_{11} + R_{12} + R_{13} \\ R_2 = R_{21} + R_{22} + R_{23} + R_{2k} \end{cases} \tag{3}$$

In a qualitative analysis of the leakage inductance, it should be noted that the permeability of nanocrystalline SMC is much lower than that of ferrite. Therefore, the magnetoresistance of the secondary magnetic circuit R_2 can be approximated as R_{2k}, and R_1/R_2 approaches zero, leading to:

$$L_k = \frac{N_1^2}{\dfrac{R_1}{R_2}\left(R_{1k} + R_2\right) + R_{1k}} \approx \frac{N_1^2}{R_{1k}} = \frac{N_1^2 \mu_0 \mu_{SMC} l_c h}{l_w} \tag{4}$$

where l_w and l_c denote the equivalent magnetic circuit length of the leakage core in radial and circumferential directions, respectively; h denotes the thickness of the leakage core; μ_0 denotes the vacuum permeability, and μ_{SMC} represents the relative permeability of the SMC core. According to the theoretical analysis, the leakage inductance of the magnetically integrated transformer is positively correlated with the permeability and the thickness of the leakage core. Specifically, the transformer leakage inductance increases when the material permeability or core thickness increases.

C. Quantitative Calculation of Leakage Inductance

The magnetically integrated transformer proposed in this study is based on a GU30 core (Silicon steel laminated core, thickness 30mm) design, whose leakage core adopts a cylindrical structure and is built inside the main core. The finite element simulation model is the complementary model shown in Fig. 2(a), and the material of the main core is PC95. To more accurately simulate the assembly state of the actual core, the simulation model is set with the following structural parameters: An air gap of 0.01 mm is retained in the sidewall splice of the main core, and an air gap of 0.2 mm is set between the leakage core and the center leg of the main core as the assembly margin.

Magnetic permeability μ_{SMC} and core thickness h are two key controllable parameters in the preparation process of SMC leakage cores. These two parameters provide design freedom for the leakage inductance regulation of magnetically integrated transformers. In this study, parametric scanning of the above parameters was carried out using the finite element analysis method. The relative permeability of the nanocrystalline SMC is set to five gradients of 1 (representing the traditional air leakage core), 5, 10, 15, and 20; meanwhile, the core thickness is parametrically analyzed in the range of 0.5 to 1.5 mm in steps of 0.01 mm. The results of the simulation calculations are shown in Fig. 3. L_n is an essential parameter in the design of the LLC converter, which represents the ratio of the transformer magnetizing inductance L_m to the resonant inductance L_r.

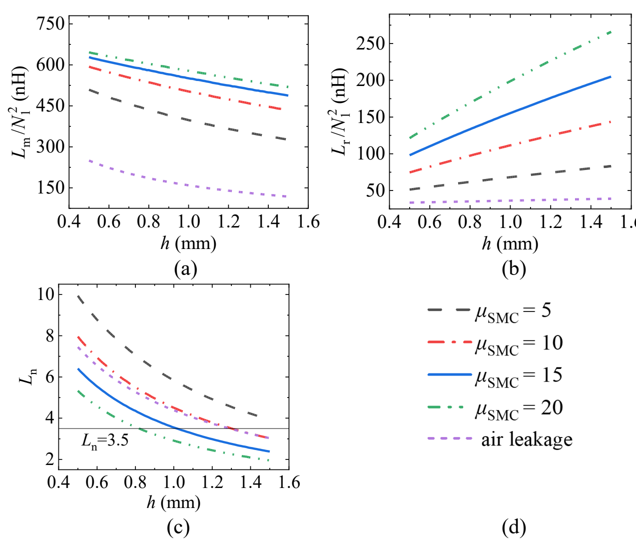

Fig. 3. The effect of leakage core permeability μ_{SMC} and thickness h on the parameters of LLC resonant circuit. (a) Magnetizing inductance per square of primary turns. (b) Resonant inductance per square of primary turns. (c) Inductance ratio. (d) Legend.

Simulation results show that increasing the thickness of the leakage core decreases L_n while increasing the leakage inductance; an increase in the permeability of the leakage core likewise increases the leakage inductance. The results of this quantitative analysis are consistent with the theoretical predictions presented earlier.

The magnetically integrated transformer designed in this study can realize any value of L_n from 2.0 to 9.9 within the given range of core parameters. Under the premise of keeping the outer dimensions of the transformer unchanged, the enhancement of the L_n value can be achieved in two ways: by reducing the thickness of the leakage core or decreasing its permeability. The former imposes stricter requirements on the magnetic powder pressing process, while the latter can effectively increase the L_n value. Still, it will also lead to a decrease in leakage inductance and magnetizing inductance. Reducing the leakage inductance necessitates a resonant capacitor with larger capacitance, whereas a decrease in magnetizing inductance increases the magnetizing current, thereby raising system losses. Based on practical engineering experience, controlling the value of L_n in the range of 2 to 5 is recommended, where 3.5 is the typical optimized value for LLC converter design.

The value of L_n is solely determined by the core geometry and is independent of the number of winding turns. While the magnitudes of L_m and L_r are related to the number of winding turns, the vertical coordinates of Figs. 3(a) and 3(b) denote the transformer magnetizing inductance or leakage inductance per square of primary turns, respectively. The results show that the transformer's magnetizing and leakage inductance values can be significantly enhanced using a high permeability leakage core under a fixed number of winding turns. In addition, increasing the thickness of the leakage core can increase the leakage inductance value, but it will decrease the magnetizing inductance. Comparative analysis shows that the leakage inductance parameter of the traditional integrated transformer with an air leakage core is less sensitive to the variation of the air gap height.

Although a higher magnetizing inductance reduces the magnetizing current, an excessively small magnetizing current may be insufficient to fully discharge the metal-oxide-semiconductor field-effect transistor (MOSFET)'s (Q_1 and Q_2 in Fig. 1) parasitic capacitance during the dead time, thus preventing zero-voltage switching (ZVS). Therefore, it is necessary to make a comprehensive trade-off between the relevant parameters in the design of the LLC converter. In Sections III and IV, the design method of the leakage core will be elaborated in detail with specific cases.

III. Modulation of Magnetic Properties of Nanocrystalline SMC

A. Mechanisms for the Regulation of Permeability

During the powder pressing process, when external pressure is applied, the magnetic powder particles will be displaced and deformed, increasing the contact area between the particles (contact is achieved through the insulating layer) and a gradual decrease in the material porosity. Theoretically, the optimal performance of SMC requires that the porosity tends to zero, at which point the material consists of only two phases, the ferromagnetic phase (magnetic powder) and the non-ferromagnetic phase (insulating layer), and the maximum magnetic permeability can be obtained. However, the actual pressing process has the following limitations: On the one hand, the complete elimination of porosity is technically challenging to realize; on the other hand, too high pressing pressures can further reduce the porosity but lead to a rupture of the insulating layer and a significant increase in the residual stresses, which deteriorates the loss characteristics of the material.

Since a porous structure is inherent to SMC, this study proposes a method to modulate material permeability by controlling the microscopic pore structure. From the microstructure point of view, an ideal SMC can be regarded as a dense ferromagnetic phase uniformly divided by an insulating layer (i.e., the gap structure). However, experimental measurements have shown that the actual billet density is often lower than the theoretical value, and microstructural analysis reveals that this discrepancy stems from the presence of pore defects within the material, as shown in Fig. 4. Under pressure, magnetic particles undergo deformation. Therefore, they are represented by rectangles in Fig. 4.

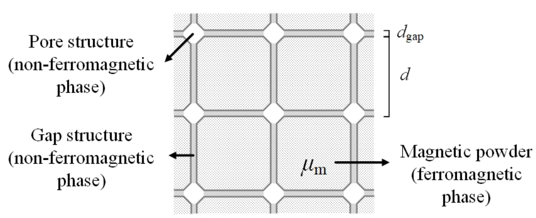

Fig. 4. SMC microstructure equivalent model.

Based on magnetic circuit analysis, the internal gaps and pores in SMC have different effects on magnetic flux: Gaps act as local high magnetic resistance areas, forming magnetic flux blockage zones and causing a sharp drop in flux density; pores cause significant distortion of the magnetic flux path, forcing the magnetic flux to form a circumferential path around them, thereby increasing the effective magnetic circuit length and magnetic resistance. Based on this, two key microstructural parameters are defined in this paper: the thickness ratio of the insulating layer, f_{gap}, and the volume fraction of pores, f_{pore}. Then, the equation for calculating the magnetic permeability μ_{SMC} of SMC can be expressed in the following form, and the derivation process can be referred to in [24]:

$$\mu_e = \frac{\mu_m}{1 - f_{gap} + \mu_m f_{gap}} \tag{5}$$

$$\mu_{SMC} = \mu_e \left[1 + \frac{3(\mu_i - \mu_e) f_{pore}}{\mu_i + 2\mu_e - (\mu_i - \mu_e) f_{pore}} \right] \tag{6}$$

where parameter μ_m denotes the relative permeability of the ferromagnetic phase in SMC. Parameter μ_e in (6), which is calculated using (5), denotes the relative permeability of the medium surrounding the pore structure. The parameter f_{gap} is a measure of the gap structure, which can be regarded as a characterization of the thickness of the insulation layer. The parameter f_{pore} characterizes the total volume fraction of pores. This microstructure is the primary reason the composite's actual density is lower than its theoretical compacted density. Parameter μ_i denotes the relative magnetic permeability inside the pores. Since it is challenging to fill pores with ferromagnetic materials using existing manufacturing processes, the relative permeability of the pore structure is set to 1 in this study.

B. Experimental Validation of the Permeability Modulation Approach

This study achieves precise control of the magnetic permeability of SMC by adjusting the thickness of the insulating layer on the surface of magnetic particles to alter the width of the gaps between them. The experiment selected phenolic resin as the insulating coating material and nanocrystalline powder of grade NC1-E as the magnetic matrix. The magnetic powder composition is FeSiBCuNb, with a relative permeability of 80,000, electrical resistivity of 130 μΩ·cm, saturation magnetic flux density of 1.25 T, and Curie temperature of 570 °C. Three parallel experimental groups were set up, with each group having a fixed magnetic powder mass of 25 g. The phenolic resin addition amounts were 1.0, 1.5, and 2.0 g, respectively, forming three control specimens with different insulation layer thicknesses. The insulation coating process details are as follows: First, dissolve phenolic resin in 20 mL of acetone solvent; subsequently, gradually add 25 g of magnetic powder to the solution in a spiral mixer; finally, complete the coating by drying the mixture. The theoretical basis for this process is detailed in [25]. The equations for calculating the gap structure width coefficient f_{gap} and the pore structure volume fraction f_{pore} are as follows:

$$f_{gap} = 1 - \left(\frac{m_2 \rho_1}{m_1 \rho_2} + 1 \right)^{-\frac{1}{3}} \tag{7}$$

$$f_{pore} = 1 - \frac{m_2 \rho_1 + m_1 \rho_2}{\rho_1 \rho_2 V_{SMC}} \tag{8}$$

where m_1 and m_2 are the masses of magnetic powder and resin, respectively; ρ_1 and ρ_2 are the densities of magnetic powder and resin, respectively; V_{SMC} is the volume of each SMC specimen. The specimens were in-house prepared, as shown in Fig. 5(a).

The static magnetic properties of the nanocrystalline SMC specimens are shown in Fig. 5(b). The measurement instrument used was a Magnet-Physik hysteresis loop measuring instrument, as shown in Fig. 5(c). Within the magnetic flux density range of less than 0.5 T, the permeability of each specimen remained highly stable, and the remanence was less than 10 mT, meeting the application requirements for high-frequency magnetic core materials in direct current (DC) converters. The specific parameters of each specimen are shown in Table I.

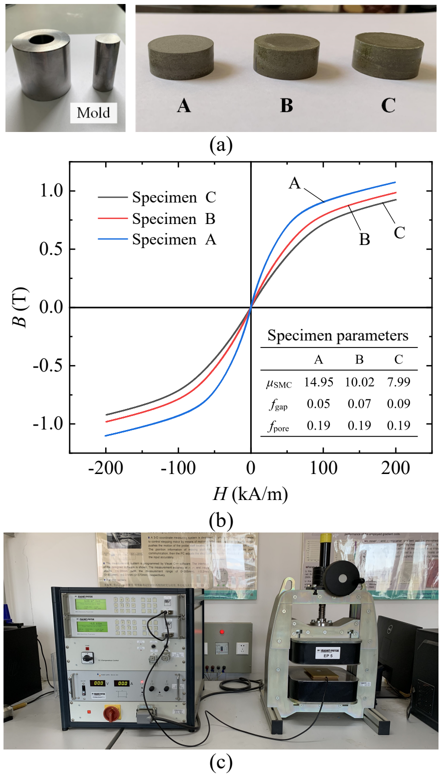

Fig. 5. Measurement of magnetic properties of SMC core specimens. (a) SMC specimens with different insulation layer thicknesses. (b) Comparison of static magnetic characteristic curves and microstructural parameters for each specimen. (c) Static magnetic characteristic measurement equipment.

TABLE I
COMPARISON OF PARAMETERS FOR EACH SPECIMEN

Parameter	Specimen		
	A	B	C
Resin content/g	1.0	1.5	2.0
Diameter of specimen/mm	25	25	25
Height of specimen/mm	10.22	10.92	11.71
Theoretical compaction density/($g\cdot cm^{-3}$)	6.39	6.07	5.80
Measured density/($g\cdot cm^{-3}$)	5.12	4.90	4.64
f_{gap}	0.05	0.07	0.09
f_{pore}	0.19	0.19	0.19
Calculated μ_e	19.72	13.79	10.81
Calculated μ_{SMC}	14.71	10.55	8.22
Measured μ_{SMC}	14.95	10.02	7.99
Permeability prediction error	1.6%	5.3%	2.9%

Taking specimen A as an example, based on the density of the nanocrystalline dense block (7.18 $g\cdot cm^{-3}$) and phenolic resin (1.7 $g\cdot cm^{-3}$), combined with the particle size of the magnetic powder (40 μm), it can be calculated that the average thickness of the magnetic powder's cladding layer is about 2.14 μm, which corresponds to the parameter f_{gap} = 0.05. According to (5), the theoretical magnetic permeability μ_e was calculated to be 19.72 (the μ_m was taken as 80,000). The theoretical compacted density of this SMC should be 6.39 $g\cdot cm^{-3}$. However, the measured density is 5.12 $g\cdot cm^{-3}$, which is different from the theoretical value attributed to the pore structure inside the material. The parameter f_{pore} = 0.19 was obtained by density analysis, and the calculated value of magnetic permeability μ_{SMC} corrected according to (6) was 14.71, with an error of only 1.61% from the measured value. Further analysis shows that the pore and gap structures in specimen A account for 20% and 14% of the total volume, respectively, but the influence of the pore structure on the permeability is significantly lower than that of the gap structure. Therefore, this study demonstrates that the method of regulating the permeability of nanocrystalline SMC by adjusting the thickness of the insulating layer is feasible.

IV. PROTOTYPE PREPARATION AND EXPERIMENTAL VERIFICATION

The LLC resonant converter designed in this study adopts a half-bridge input and full-bridge rectifier output structure. The schematic diagram is shown in Fig. 1, and the design specifications are shown in Table II.

TABLE II
DESIGN SPECIFICATIONS OF LLC RESONANT CONVERTER

Parameter	Value
Input voltage range/V	380–400
Output voltage/V	40
Rated output power/W	200
Rated output current/A	5
Full load efficiency requirement	> 95%
Operating frequency range/kHz	90–120

Setting the converter at an input voltage of 390 V when the voltage gain M_g is 1, the diode voltage drop V_F is about 0.55 V (Schottky diode), then the transformer turns ratio n calculated according to (9) is about 4.74. However, accounting for losses in both the MOSFET and the transformer, the actual turns ratio n is chosen to be slightly less than 4.74.

$$n = \frac{M_g V_{in}}{2\left(V_o + 2V_F\right)} \tag{9}$$

where V_{in} and V_o denote the input and output voltages of the converter, respectively.

According to (10), the calculated resonant capacitance value should be 22.5 nF, which is the actual choice of a 22 nF MMKP82 capacitor. In this equation, R_e represents the equivalent load resistance, approximately 149.4 Ω. Q_e denotes the quality factor, initially set to 0.45. f_r is the resonant frequency generated by the resonant capacitor C_r and leakage inductance, initially set to 105 kHz.

$$C_r = \frac{1}{2\pi Q_e f_r R_e} \tag{10}$$

The value of resonant inductance (transformer leakage inductance) calculated according to (11) should be 104.4 μH. L_n is taken to be 3.5, then the magnetizing inductance of the transformer is designed to be 365.4 μH.

$$L_r = \frac{1}{\left(2\pi f_r\right)^2 C_r} \tag{11}$$

The prototype employs a GU30 standard pot-core ferrite with PC95 material, as introduced previously. As this core has a continuous center leg (no air gap), the ferrite core was machined using three-dimensional (3D) engraving to create a recess for mounting the SMC leakage core. The ferrite core's inner diameter measures about 25.10 mm. The fabricated SMC leakage core has an outer diameter of 25.00 mm, enabling it to be inserted into the ferrite core with a deliberate clearance margin against the sidewalls. During assembly, thermally conductive silicone adhesive was applied within the transformer structure to secure the SMC leakage core in place.

If the relative permeability of the leakage core is designed as 20, the fabricated core thickness should be 0.82 mm. When the permeability is adjusted to 15, 10, or 5, the corresponding thickness increases to 1.02, 1.30, and 1.67 mm, respectively. Based on prior calculations, the required magnetizing inductance for the transformer is 365.4 μH. Additionally, integral turns are necessary for both primary and secondary windings to facilitate winding. Considering these factors, the relative permeability of the leakage core is ultimately set to 10 with a thickness of 1.30 mm, using a winding configuration of 28 primary turns and 6 secondary turns.

This study also compares the loss performance of the in-house prepared nanocrystalline SMC (FeSiBCuNb) with various commercial SMCs (FeSi, FeSiNi, FeSiAl, and FeNi) at a frequency of 100 kHz, with results shown in Fig. 6. The maximum operating magnetic flux density of this material in integrated transformer is approximately 0.1 T. Material loss testing was conducted according to IEC 60404-6 standards using the ring specimen method, with target ring specimen fabrication parameters consistent with specimen B in Table I. Results indicate that the prepared nanocrystalline SMC exhibits the lowest loss.

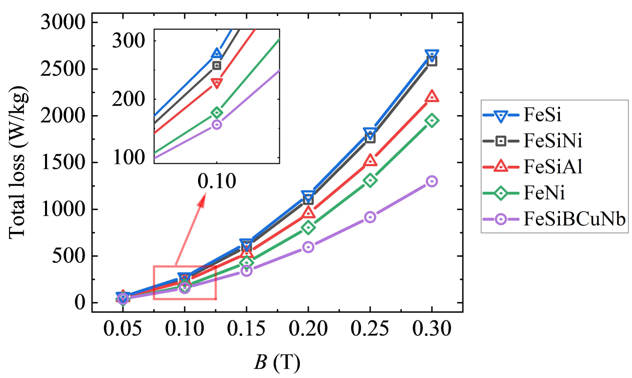

Fig. 6. Loss comparison between prepared nanocrystalline SMC and other SMCs (excitation frequency 100 kHz)

Additionally, this study measured the relative permeability (μ_{SMC}), remanence (B_r), and coercivity (H_c) of the nanocrystalline SMC under different frequencies and temperatures; the results are summarized in Table III. At different temperatures, although the magnetic permeability of FeSiBCuNb material itself is affected by temperature, the inherent micro-gap structure of SMC mitigates changes in the material's macroscopic magnetic properties caused by variations in magnetic powder performance, as described by (5). At different frequencies, the primary cause of variations in coercivity and remanence is the influence of eddy currents within the material. However, at the rated operating frequency, eddy current losses account for only 7% of the total losses. Consequently, the frequency stability and temperature stability of the magnetization characteristics of nanocrystalline SMC both meet application requirements.

TABLE III
MAGNETIC PROPERTIES OF NANOCRYSTALLINE SMC AT DIFFERENT TEMPERATURES AND FREQUENCIES ($B = 0.1$ T)

Test environment temperature/°C	Frequency/ kHz	μ_{SMC}	B_r/T	H_c/(A·m^{-1})
25	50	10.03	0.0016	132
25	100	10.02	0.0017	135
25	150	9.99	0.0017	137
100	50	10.05	0.0016	128
100	100	10.03	0.0016	132
100	150	10.01	0.0017	134

Finite element simulations conducted in Ansys confirm that this design yields a magnetizing inductance of 360.2 μH and a leakage inductance of 102.9 μH, meeting the design specifications. For the power switch, the NCE65T1K2K is selected. Calculations indicate that a dead time exceeding 10 ns is required to achieve ZVS; therefore, the EG2104 half-bridge driver is implemented. The final fabricated LLC resonant converter validation circuit is shown in Fig. 7, which illustrates the decomposition structure of the magnetically integrated transformer.

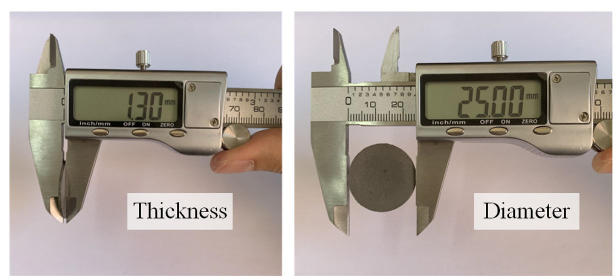

(a)

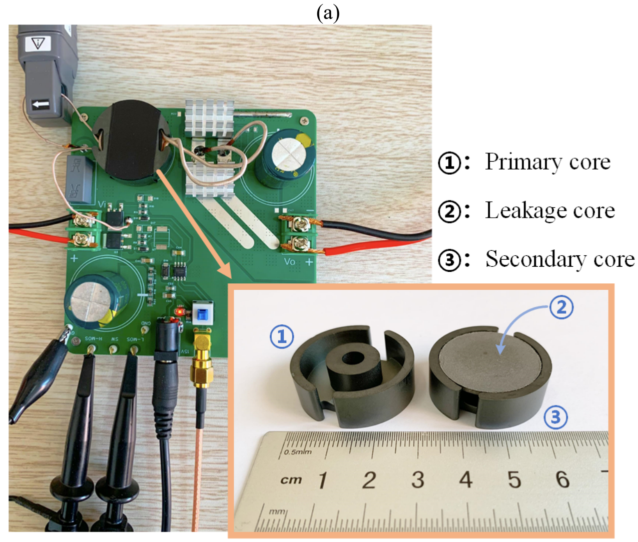

(b)

Fig. 7. Test circuit for magnetically integrated transformer. (a) SMC leakage core size. (b) LLC resonant converter prototype.

Using an impedance analyzer, this study measured the magnetizing inductance L_m of 369.6 μH and the leakage inductance L_r of 106.5 μH for the integrated transformer. The parameter L_n was calculated as 3.47, aligning with the design target. Under full-load conditions with an input voltage of 389.10 V and a switching frequency of 110 kHz, the LLC resonant converter achieved an output voltage of 40.15 V, delivering 201.5 W. The measured input current was 0.54 A, corresponding to an efficiency of 95.9%, thereby satisfying the design specifications. The primary-side voltage and current waveforms of the transformer are presented in Fig. 8. Calculations based on circuit parameters indicate an actual resonant frequency f_r of approximately 104 kHz, confirming operation above resonance.

The efficiency of the converter under different power output conditions and the proportion of SMC leakage core losses in total losses are shown in Fig. 9. Under full-load output conditions, the SMC core has a loss of approximately 0.22 W, while the total core loss of the transformer is about 0.95 W.

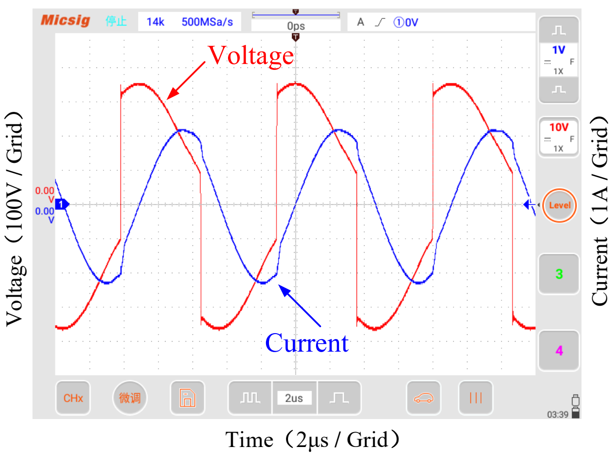

Fig. 8. Integrated transformer primary winding voltage and current waveforms.

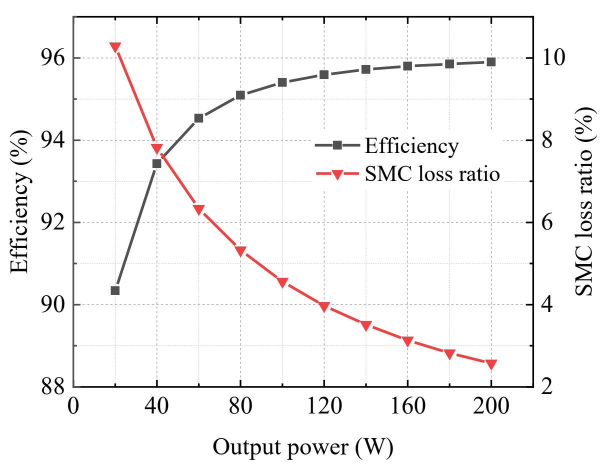

Fig. 9. Efficiency curve of LLC converter and loss proportion of SMC core.

This study further compares the key parameter differences between the proposed magnetically integrated transformer and a conventional air-core leakage inductance transformer (both sharing identical physical dimensions). For the conventional air-core design, achieving the same inductance ratio L_n requires a total air gap width of 1.48 mm. To attain a comparable magnetizing inductance L_m, its primary winding necessitates 52 turns. The transformers are depicted in Fig. 10. Measurements confirm a magnetizing inductance of 367.4 μH for the conventional design. Due to the increased turn count and the constraint of maintaining a similar window utilization factor, the conventional design requires finer Litz wire for the primary winding. Consequently, its allowable primary root mean square (RMS) current is significantly reduced.

To validate the performance disparity, the conventional air leakage core transformer was implemented in the same LLC resonant converter circuit. While maintaining nearly identical circuit parameters (output voltage remained at 40 V), the load resistance had to be adjusted to 22 Ω to ensure normal operation due to the transformer's limitations. Table IV details the comparative parameters of both transformers. The magnetizing current was determined by difference calculations of synchronously captured primary and secondary currents. Experimental results demonstrate that the input active power on the primary side of the proposed SMC leakage core integrated transformer reaches approximately 2.5 times that of the conventional design.

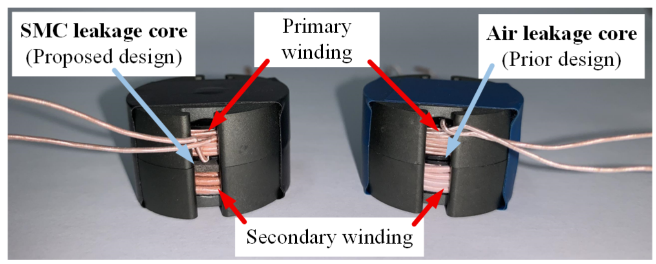

Fig. 10. The proposed integrated transformer design and prior design.

TABLE IV
COMPARISON BETWEEN SMC LEAKAGE CORE AND AIR LEAKAGE CORE MAGNETICALLY INTEGRATED TRANSFORMERS

Parameters		SMC leakage core	Air leakage core
Primary winding	Litz wire specifications	0.1 × 40	0.1 × 25
	Turns	28	52
	Window area/mm^2	40.87	40.87
	Window utilization factor	50.6%	49.0%
Secondary winding	Litz wire specifications	0.1 × 140	0.1 × 70
	Turns	6	11
	Window area/mm^2	31.72	32.03
	Window utilization factor	45.0%	42.1%
Operating	Frequency/kHz	110	109
	Primary RMS voltage/V	263.1	246.3
	Primary RMS current/A	1.513	0.946
	RMS magnetizing current/A	0.664	0.683
Active power input at primary side/W		206.9	84.5

This study selected GU series pot-core ferrites as the experimental material, primarily for two reasons. First, their circumferentially symmetric geometry effectively suppresses interference from winding leakage flux on circuit parameter measurements, ensuring accurate validation of the feasibility principle for SMC leakage core transformer. Second, although PQ and EE series cores are more prevalent in power circuits, they exhibit equivalent magnetic circuit structures to the GU series. Consequently, the methodology proposed in this study is equally applicable to these core types.

For example, the structure of magnetically integrated transformers in the PQ and EE series is shown in Fig. 11. As illustrated in Fig. 3(c), when both the permeability and thickness of the leakage core are set to their minimum values, the transformer's L_n value reaches its maximum; conversely, when both are set to their maximum values, the L_n value reaches its minimum. Within this range, the L_n value exhibits a monotonic variation trend with changes in permeability and thickness. Therefore, simulations were conducted for both extreme cases mentioned above. The calculated transformer parameters under these conditions are presented in Table V. During converter design, if the required transformer parameters fall between these two extreme states, adaptive modifications to the magnetically integrated transformer can be achieved by fabricating SMC cores with corresponding shapes.

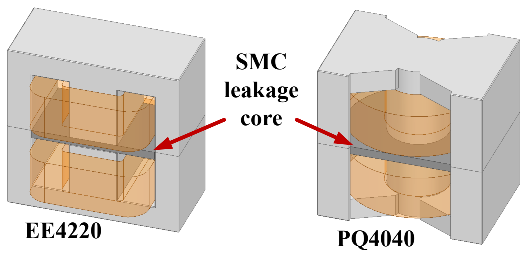

Fig. 11. Structure of magnetically integrated transformers in the EE and PQ core series (ferrite component grade: PC95).

TABLE V
PARAMETERS OF MAGNETICALLY INTEGRATED TRANSFORMERS WITH EE CORE AND PQ CORE

Core model	EE4220	EE4220	PQ4040	PQ4040
h/mm	1	3	1	3
μ_{SMC}	5	20	5	20
L_n	9.80	2.77	8.27	2.01
Single-turn magnetizing inductance/nH	805.5	768.34	630.47	598.04
Single-turn resonant inductance/nH	82.16	276.96	76.26	297.72
Primary side window area/mm^2	137.8	137.8	153.4	153.4
Secondary side window area/mm^2	128.7	110.4	142.9	121.9

V. CONCLUSION

This study proposes a novel integrated transformer that employs a nanocrystalline SMC leakage core to improve upon conventional air-core designs. The permeability of this material is tunable during fabrication, enabling precise control over the shunting ratio of the main magnetic flux. This facilitates accurate adjustment of the leakage inductance parameter. Furthermore, this design achieves a magnetizing inductance comparable to traditional air leakage core transformers but with fewer winding turns. Consequently, larger cross-sectional area conductors can be used for both primary and secondary windings, significantly enhancing the transformer's power density. Experimental results demonstrate that the proposed integrated transformer with the nanocrystalline SMC leakage core achieves an input active power approximately 2.5 times higher than the conventional design. This technology holds promise for application in power adapters for portable electronics, such as laptops and mobile phones, to improve their power density.

REFERENCES

[1] F. Jin, T. L. Yuan, and A. Nabih *et al.*, "Efficient Integrated Magnetics with Winding Cancellation Technique to Reduce Common-mode EMI Noise for a Single-phase CLLC Converter," *IEEE Trans. on Power Electron.*, vol. 39, no. 11, pp. 14758–14774, Nov. 2024.

[2] J. Y. Bao, Y. Li, and B. Y. Liu *et al.*, "Three-phase Interleaved Bidirectional LLC Resonant Converter with Vertically Integrated Magnetics for Energy Storage System Applications," *IEEE Trans. on Power Electron.*, vol. 40, no. 4, pp. 5371–5383, Apr. 2025.

[3] A. E. Shafei, S. Ozdemir, and N. Altin *et al.*, "Development of a Medium Voltage, High Power, High Frequency Four-port Solid State Transformer," *CES Trans. on Electr. Mach. and Syst.*, vol. 6, no. 1, pp. 95–104, Mar. 2022.

[4] Y. Liu, H. F. Wu, and S. Ni *et al.*, "Lower-height-oriented Magnetic Integration Design for Onboard Power Converter of Electric Vehicles," *IEEE Trans. on Transp. Electrif.*, vol. 10, no. 1, pp. 163–173, Mar. 2024.

[5] R. Gadelrab, and F. C. Lee, "PCB-based Magnetic Integration and Design Optimization for Three-phase LLC," *IEEE Trans. on Power Electron.*, vol. 38, no. 11, pp. 14037–14049, Nov. 2023.

[6] F. Li, L. L. Wang, and L. Y. Yu, "A Novel Integrated Matrix Magnetics for Isolated Single-stage DC–DC Converter," *IEEE Trans. on Power Electron.*, vol. 37, no. 10, pp. 12380–12390, Oct. 2022.

[7] J. L. Zheng, Z. M. Zhao, and B. C. Shi *et al.*, "A Discrete State Event Driven Simulation based Losses Analysis for Multi-terminal Megawatt Power Electronic Transformer," *CES Trans. on Electr. Mach. and Syst.*, vol. 4, no. 4, pp. 275–284, Dec. 2020.

[8] L. Chen, L. S. Cui, and T. Ben *et al.*, "An Improved Preisach Distribution Function Identification Method Considering the Reversible Magnetization," *CES Trans. on Electr. Mach. and Syst.*, vol. 7, no. 4, pp. 351–357, Dec. 2023.

[9] Y. F. Wang, C. Chen, and B. Chen *et al.*, "Optimal Design of Transformer Winding of LLC Converter," *Transactions of China Electrotechnical Society*, vol. 37, no. 5, pp. 1252–1261, Mar. 2022.

[10] Y. Q. Lv, F. J. Deng, and Z. Shen *et al.*, "Quad-port Magnetic Integrated Coupled Inductor Based Magnetic Network Energy Routers with High Power Density," *IEEE Trans. on Power Electron.*, vol. 40, no. 8, pp. 11655–11672, Aug. 2025.

[11] H. Cheng, P. S. Li, and K. Xu *et al.*, "Fully Integrated Magnetic Structure and Optimized Design of Dual Buck-boost-CLLC Three-port Converter," *Transactions of China Electrotechnical Society*, vol. 40, no. 10, pp. 3209–3223, May 2025.

[12] M. H. Jiang, Q. F. Wu, and Q. Wang *et al.*, "Integrated Optimization Design of LLC Four-element-matrix Planar Transformer Considering Loss and Parasitic Parameters," *Transactions of China Electrotechnical Society*, vol. 40, no. 10, pp. 3195–3208, May 2025.

[13] Y. Liu, H. F. Wu, and J. Zou *et al.*, "CLL Resonant Converter with Secondary Side Resonant Inductor and Integrated Magnetics," *IEEE Trans. on Power Electron.*, vol. 36, no. 10, pp. 11316–11325, Oct. 2021.

[14] C. W. Park, and S. K. Han, "Analysis and Design of an Integrated Magnetics Planar Transformer for High Power Density LLC Resonant Converter," *IEEE Access*, vol. 9, pp. 157499–157511, Nov. 2021.

[15] A. Lordoglu, M. O. Gulbahce, and S. Dusmez, "Integrated Planar Magnetics Optimization for Δ−Δ LLC Converter with Wide Output Voltage Range," in *Proc. of 2024 IEEE Applied Power Electronics Conference and Exposition (APEC)*, Long Beach, CA, USA, Feb. 2024, pp. 1746–1753.

[16] Y. F. Wang, C. Chen, and B. Chen *et al.*, "A Magnetic Integrated Method for Noise Suppression based on Input Series Output Parallel LLC," *Transactions of China Electrotechnical Society*, vol. 37, no. 9, pp. 2319–2328, May 2022.

[17] H. Cheng, K. Xu, and P. S. Li *et al.*, "Design and Optimization of Three-phase CLLC Resonant Converter with Magnetic Integrated Planar Transformer," *Transactions of China Electrotechnical Society*, vol. 39, no. 12, pp. 3774─3786, Jun. 2024.

[18] K. Sun, S. L. Lu, and Z. Y. Yi *et al.*, "A Review of High-power High-frequency Transformer Technology for Power Electronic Transformer Applications," *Proceedings of the CSEE*, vol. 41, no. 24, pp. 8531─8545, Dec. 2021.

[19] M. X. Li, Z. W. Ouyang, and M. A. E. Andersen, "High-frequency LLC Resonant Converter with Magnetic Shunt Integrated Planar Transformer," *IEEE Trans. on Power Electron.*, vol. 34, no. 3, pp. 2405─2415, Mar. 2019.

[20] S. A. Ansari, J. N. Davidson, and M. P. Foster, "Inserted-shunt Integrated Planar Transformer with Low Secondary Leakage Inductance for LLC Resonant Converters," *IEEE Trans. on Ind. Electron.*, vol. 70, no. 3, pp. 2652─2661, Mar. 2023.

[21] C. C. Liu, Z. Chao, and S. P. Wang *et al.*, "Design and Performance Analysis of Permanent Magnet Claw Pole Machine with Hybrid Cores," *CES Trans. on Electr. Mach. and Syst.*, vol. 7, no. 3, pp. 275─283, Sept. 2023.

[22] C. C. Liu, F. Yang, and W. F. Zhang *et al.*, "Design Optimization of a Novel Axial-radial Flux Permanent Magnet Claw Pole Machine with SMC Cores and Ferrite Magnets," *CES Trans. on Electr. Mach. and Syst.*, vol. 7, no. 4, pp. 358─365, Dec. 2023.

[23] D. Grybos, J. Leszczynski, and C. Swieboda *et al.*, "Magnetic Properties of Composite Cores Made of Nanocrystalline Material for High Frequency Inductors and Transformers," in *Proc. of 2018 Innovative Materials and Technologies in Electrical Engineering (i-MITEL)*, Sulecin, Poland, Apr. 2018, pp. 1─6.

[24] K. M. Shi, D. H. Zhang, and Z. Y. Ren *et al.*, "Evaluation of Equivalent Permeability of Soft Magnetic Composites Considering Manufacturing Process," *IEEE Trans. on Magn.*, vol. 59, no. 5, pp. 1─4, May 2023.

[25] A. H. Taghvaei, H. Shokrollahi, and A. Ebrahimi *et al.*, "Soft Magnetic Composites of Iron-phenolic and the Influence of Silane Coupling Agent on the Magnetic Properties," *Mater. Chem. and Phys.*, vol. 116, no. 1, pp. 247─253, Jul. 2009.

Kaimeng Shi was born in Liaoning, China, in 1995. He received the B.E. degree and M.E. degree in Electrical Engineering from Shenyang University of Technology, Shenyang, China, in 2017 and 2020. He is pursuing a Ph.D. degree in electrical engineering from Shenyang University of Technology. His current research interests include the modeling of novel magnetic materials and their applications in the field of power electronics.

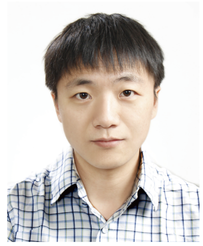

Dianhai Zhang (S' 11–M' 13) He received his B.S. and M.S. degrees in biomedical engineering, electrical machine, and electric apparatus from Shenyang University of Technology Shenyang, China, in 2006 and 2009, respectively, and Ph.D. degree in electrical engineering from Chungbuk National University Chungbuk, Korea, in 2013. He is presently a professor at the School of Electrical Engineering, Shenyang University of Technology, China. His research interests include the measurement and modeling of magnetic properties of novel magnetic materials and multi-physical field coupling analysis of electrical equipment.

Xuanzhe Zhao was born in Inner Mongolia Autonomous Region, China, in 1998. He received the B.E. degree in Electrical Engineering and Automation from Jilin University of Chemical Technology, Jilin, China, in 2020, and the M.E. degree in electrical engineering from Shenyang University of Technology, Shenyang, China, in 2024. He is pursuing a Ph.D. degree in electrical engineering from Shenyang University of Technology, Shenyang, China. His current research interests include magnetic property measurement and simulation of electrical engineering materials, as well as structural characterization and analytical prediction of magnetic properties of soft magnetic composites.

Ziyan Ren (S' 11–M' 13) received her B.S degree and M.S degree from Shenyang University of Technology, China, in 2006 and 2009, respectively. She received the Ph.D. degree in Electrical Engineering from Chungbuk National University, Chungbuk, Korea in 2013. She is currently a professor in Shenyang University of Technology, Shenyang, China. Her research interests include the optimal design of electro-magnetic devices and the numerical analysis of electromagnetic fields.